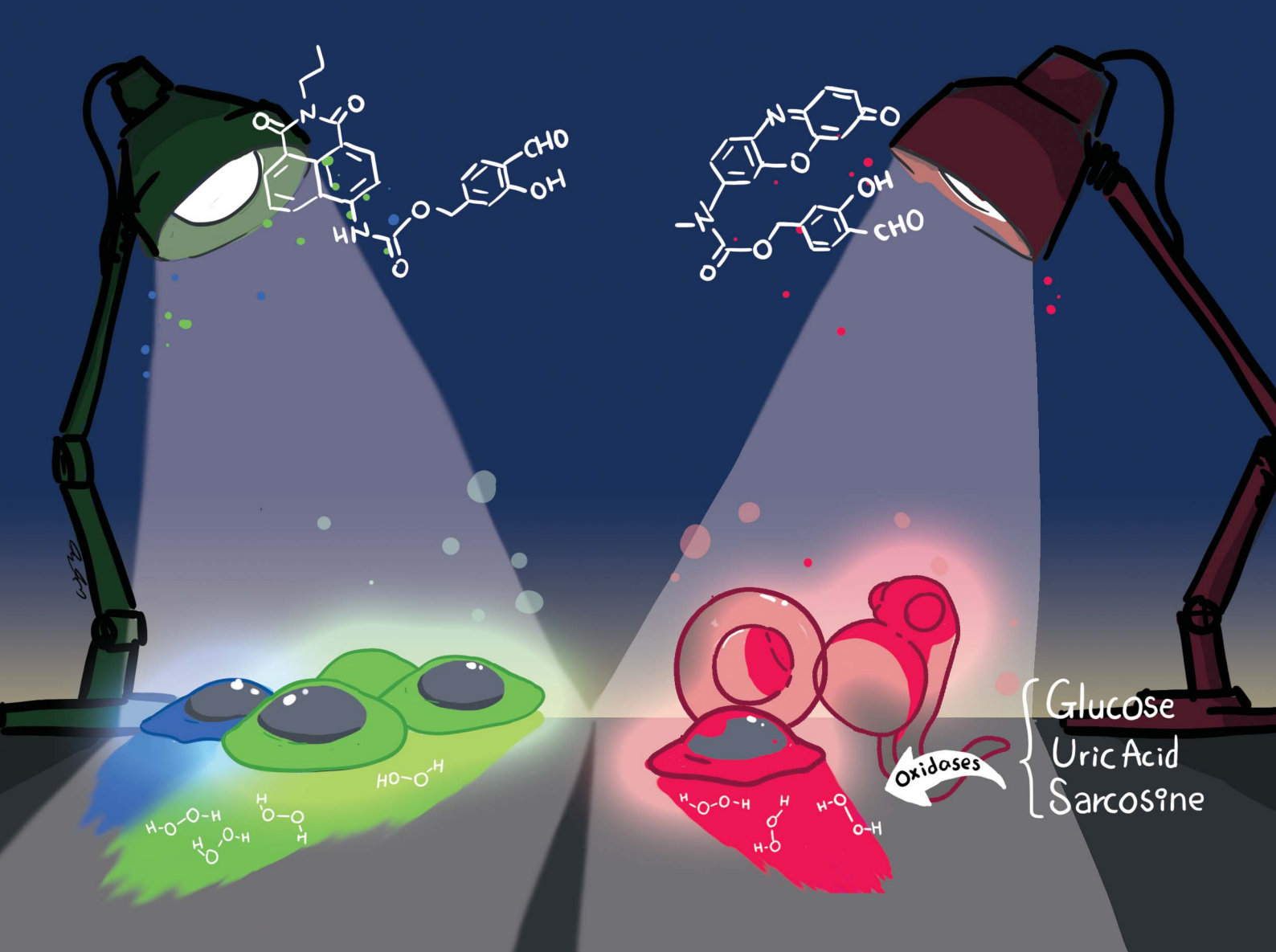


Chemical Science

rsc.li/chemical-science



ISSN 2041-6539



Cite this: *Chem. Sci.*, 2020, **11**, 11989

All publication charges for this article have been paid for by the Royal Society of Chemistry

Received 4th September 2020
Accepted 27th September 2020

DOI: 10.1039/d0sc04888g

rsc.li/chemical-science

Fluorescent probes for *in vitro* and *in vivo* quantification of hydrogen peroxide†

Sen Ye, Jun Jacob Hu, Qian Angela Zhao and Dan Yang *

Hydrogen peroxide (H_2O_2) plays essential roles in redox signaling and oxidative stress, and its dynamic concentration is critical to human health and diseases. Here we report the design, syntheses, and biological applications of **HKPerox-Red** and **HKPerox-Ratio** for quantitative measurement of H_2O_2 . Both probes were successfully applied to detect endogenous H_2O_2 fluxes in living cells or zebrafish, and biological effects of multiple stress inducers including rotenone, arsenic trioxide, and starvation were investigated. As H_2O_2 is a common by-product for oxidase oxidation, a general assay was developed for ultrasensitive detection of various metabolites (glucose, uric acid, and sarcosine). Moreover, cellular H_2O_2 measurements were achieved for the first time by combining flow cytometry with live cell calibration. This study provides a pair of unique molecular tools for advanced H_2O_2 bio-imaging and assay development.

Introduction

Oxygen fuels energy production processes in aerobic organisms through respiration, while partial reduction of oxygen produces reactive oxygen species (ROS) as by-products of oxygen metabolism.¹ Among all ROS, hydrogen peroxide (H_2O_2) stands out as the most significant messenger molecule for redox signaling due to its relatively long half-life and diffusion range.² Cellular H_2O_2 is constantly produced with a steady-state concentration ($\sim 0.1 \mu M$) to signal cell growth and proliferation, whereas higher levels of H_2O_2 (e.g. $\sim 100 \mu M$) trigger cell growth arrest or apoptosis.^{2b,3} Quantitative analysis of H_2O_2 in biological content is key to understanding its multiple roles in redox signaling and oxidative stress. However, there is no method currently available for non-invasive, sensitive, and precise measurement of H_2O_2 in intact cells, and previous H_2O_2 quantifications relied heavily on electrochemical analysis or peroxidase-based H_2O_2 assay, where only extracellular H_2O_2 secreted from cells could be measured accurately.⁴

A powerful tool to investigate cellular H_2O_2 fluxes is fluorimetry (e.g. confocal imaging and flow cytometry) due to its high sensitivity, non-invasiveness and spatio-temporal resolution.^{5,6} While several genetically encoded H_2O_2 sensors have been developed for H_2O_2 detection with unparalleled dynamic subcellular precision, they may suffer from pH sensitivity, poor

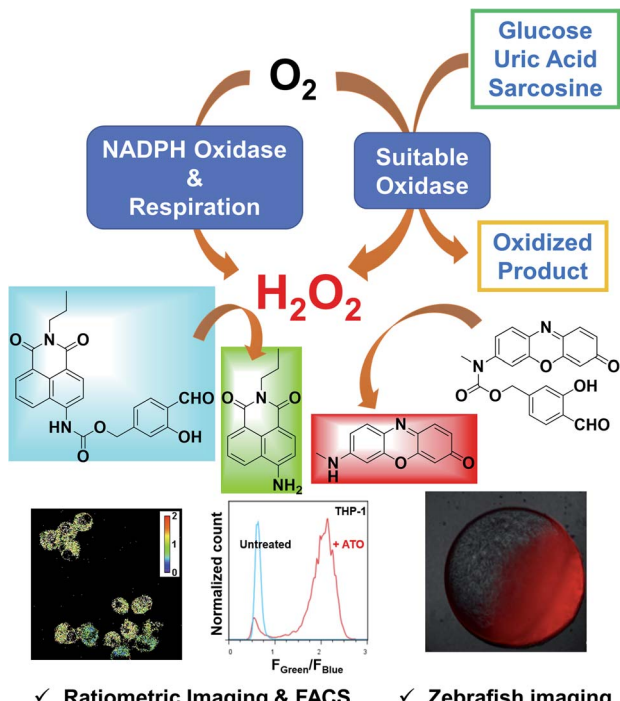
brightness, limited responses and selectivity toward H_2O_2 .⁷ Nearly all chemosensors for H_2O_2 detection are based on small-molecule dyes, including traditional dichloro-dihydro-fluorescein diacetate (DCFH-DA, a commonly used unselective ROS probe) and selective probes, especially activity-based sensing,^{5c} including boronate oxidation,^{5a,8} Baeyer–Villiger reaction,^{5b,9} tandem Payne/Dakin reaction,¹⁰ and very recently Mislow–Evans rearrangement.¹¹ Those intensity-based probes are very sensitive, but they are prone to signal fluctuations arising from variations in probe uptake, distribution, or even optical inputs. Therefore, ratiometric sensing with an internal standard for calibration is more desirable for quantitative measurement of H_2O_2 ,¹² however, most of current ratiometric probes (including both biosensors and chemosensors) still suffer from low selectivity, low sensitivity, as well as slow response, thereby limited biological applications.^{7,13}

To address those challenges, we herein report a pair of new fluorescent probes, **HKPerox-Red** and **HKPerox-Ratio** (Scheme 1). Both probes feature excellent selectivity and sensitivity for unambiguous H_2O_2 detection and quantification in aqueous solution. Moreover, the red emissive **HKPerox-Red** allows imaging endogenous H_2O_2 fluxes in living cells and zebrafish embryos, by virtue of its outstanding permeability. **HKPerox-Red** was further utilized to develop a general *in vitro* assay for ultrasensitive detection of various biomarkers and respective oxidases (glucose/glucose oxidase, uric acid/urate oxidase, sarcosine/sarcosine oxidase), since H_2O_2 is quantitatively produced during those enzymatically catalyzed oxidation reactions. As a result of its nanomolar sensitivity, **HKPerox-Red** could be used for accurate measurement of glucose with 1000 times diluted serum (1 μL to 1 mL), which provides a new method for non-invasive glucose detection with high precision.

Department of Chemistry, Morningside Laboratory for Chemical Biology, The University of Hong Kong Shenzhen Institute of Research and Innovation (HKU-SIRI), The University of Hong Kong, Pokfulam Road, Hong Kong, P. R. China. E-mail: yangdan@hku.hk

† Electronic supplementary information (ESI) available: Experiment details, including general methods, synthetic details, kinetic study, toxicity study and supplemental figures. See DOI: 10.1039/d0sc04888g





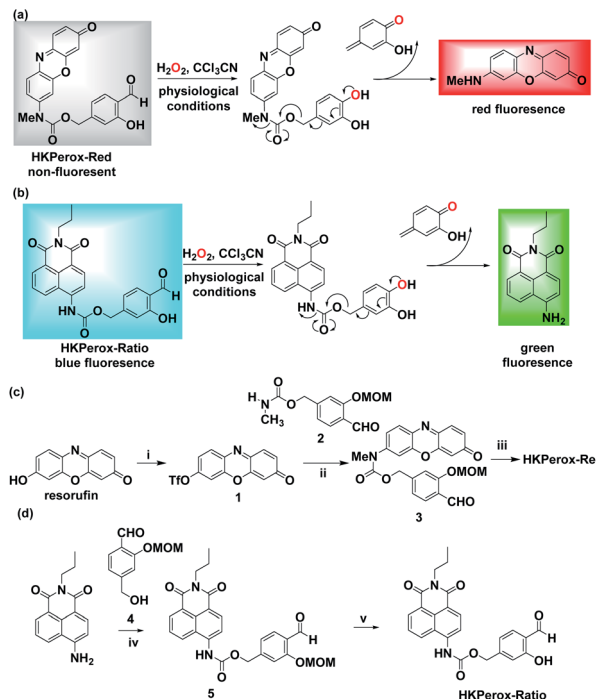
Scheme 1 HKPerox-Red and HKPerox-Ratio for H_2O_2 bio-imaging and *in vitro* assay development.

On the other hand, our novel ratiometric probe **HKPerox-Ratio** has been successfully applied to detect H_2O_2 burst induced by arsenic trioxide (As_2O_3) in multiple leukaemia cell lines. For the first time, intracellular H_2O_2 in response to starvation is visualized and quantified with **HKPerox-Ratio** by using both confocal microscopy and flow cytometry, establishing a useful protocol for H_2O_2 ratiometric analysis with spatio-temporal precision. Our new data confirm the value of **HKPerox** series for advanced bio-imaging analysis (*in vivo* imaging, ratiometric imaging, and flow cytometry analysis) as well as the development of ultrasensitive chemical tools to interrogate H_2O_2 -related physiology and pathology.

Results and discussion

Design and synthesis of HKPerox-Red and HKPerox-ratio

Our general strategy on developing red emissive and ratiometric H_2O_2 probes is based on modulation of internal charge transfer (ICT) of fluorophores that could be deprotected upon H_2O_2 mediated Payne/Dakin reaction (activity-based sensing). As shown in Schemes 1 and 2a, an electron-withdrawing carbamate sensing moiety could efficiently interrupt the ICT process in the resorufin derivative, making **HKPerox-Red** essentially non-fluorescent. However, after H_2O_2 -mediated deprotection, the remaining electron-donating 7-methylamino group could restore the push-pull conjugating system in 3*H*-phenoxyazin-3-one scaffold, releasing a bright red emission. Similarly, **HKPerox-Ratio** was designed by modulating ICT on a biocompatible 4-amino-1,8-naphthalimide platform (see Scheme 2b):^{12a,14} before the treatment of H_2O_2 , the electron-withdrawing



Scheme 2 Design and synthesis of HKPerox-Red and HKPerox-Ratio. Rational design of (a) HKPerox-Red and (b) HKPerox-Ratio for H_2O_2 sensing based on tandem Payne/Dakin reaction. Synthetic schemes for (c) HKPerox-Red and (d) HKPerox-Ratio. Reagents and conditions: (i) DMF, NaH , PhNTf_2 , 0°C , 8 h, 74%; (ii) $\text{Pd}_2(\text{dba})_3$, xantphos, Cs_2CO_3 , dioxane, 100°C , 24 h, 57%; (iii) TFA/DCM ($v/v = 1:1$), rt, 2 h, 95%; (iv) DIPEA, triphosgene, toluene, reflux, 1 h; 1, DCM , rt, 3 h, 38%; (v) TFA/DCM ($v/v = 1:1$), rt, 2 h, 92%.

carbamate linker on the 4-position of 1,8-naphthalimide disrupts the ICT process to produce a blue emission; upon H_2O_2 mediated deprotection, the carbamate linker is efficiently cleaved to release the electron-donating amine, and the ICT process is restored to provide a bright green emission.

Two general synthetic routes were envisioned to prepare **HKPerox-Red** and **HKPerox-Ratio**: (1) a general coupling reaction between halogen- or triflate-substituted fluorophores and the carbamate sensing moiety; (2) a general addition reaction between isocyanate-substituted fluorophores and the benzyl alcohol sensing moiety. Specifically, **HKPerox-Red** was synthesized from commercially available resorufin in three steps: triflation, a cross-coupling between triflate 1 and carbamate 2, and deprotection. **HKPerox-Ratio** was synthesized according to another approach (Scheme 2d) for amine-containing fluorophore: 4-amino group of 1,8-naphthalimide fluorophore was first converted to an isocyanate by treatment with triphosgene, and the *in situ* generated isocyanate readily reacted with the benzyl alcohol sensing moiety 4 to form carbamate 5, which was deprotected to afford **HKPerox-Ratio**.

Reactivity and selectivity of HKPerox-Red and HKPerox-Ratio toward H_2O_2

With both probes in hand, we first investigated the spectroscopic properties of **HKPerox-Red** and **HKPerox-Ratio** in



potassium phosphate buffer (0.1 M, pH 7.4, 100 μ M CCl_3CN). Due to its excellent water-solubility, both probes could form a homogenous solution in the buffer without additional cosolvent. As shown in Fig. 1a, an obvious absorption peak of **HKPerox-Red** was observed at 580 nm after H_2O_2 treatment. At the same time, a bright red emission at 602 nm appeared with increasing amounts of H_2O_2 in a dose-dependent manner (0–100 μ M). The resulting fluorescent product was detected as a resorufin derivative by UPLC-MS analysis (Scheme 2a and ESI†), which confirms that tandem Payne/Dakin reaction was successfully extended to this scaffold. As shown in Fig. 1c, the fluorescence intensity at 602 nm was linearly correlated with H_2O_2 concentration ranging from 0 to 30 μ M. The detection limit was estimated to be as low as 4.8 nM ($3\sigma/k$) with this standard calibration curve, which could be used as an ultra-sensitive assay for H_2O_2 quantification. The major challenges for H_2O_2 sensors are actually sensitivity and selectivity: the reactivity of H_2O_2 is milder than those highly reactive species, thus competing responses from other ROS seem to be inevitable with previously reported strategies. However, **HKPerox-Red** is highly sensitive toward H_2O_2 , and a >150-fold enhancement in fluorescence intensity was observed upon treatment with H_2O_2 , while other potential competing ROS/RNS including $^1\text{O}_2$, ROO^\cdot , TBHP, NO , O_2^\cdot , $\cdot\text{OH}$, ONOO^\cdot , and HOCl , only triggered negligible changes (Fig. 1d).

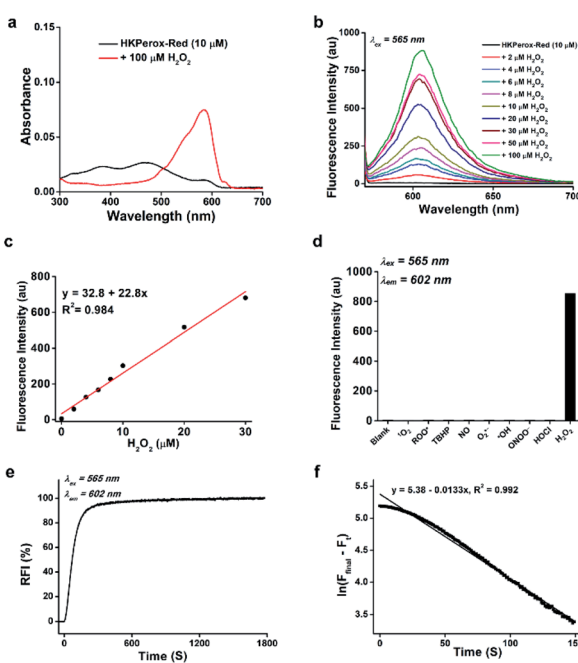


Fig. 1 Chemical characterization of **HKPerox-Red** (10 μ M) in 0.1 M potassium phosphate buffer (pH 7.4, 0.5% DMF, 100 μ M CCl_3CN). (a) Absorbance spectra of **HKPerox-Red** before and after treatment with H_2O_2 (100 μ M). (b) Fluorescence emission spectra of **HKPerox-Red** upon treatment with different amounts of H_2O_2 (0–100 μ M). (c) Fluorescence intensity of **HKPerox-Red** at 602 nm as a function of H_2O_2 (0–30 μ M). (d) Fluorescence responses of **HKPerox-Red** toward various reactive oxygen/nitrogen species (ROS/RNS; 100 μ M). (e) Time course of **HKPerox-Red** (1 μ M) in buffer treated with 1 mM H_2O_2 . (f) Rate calculation based on pseudo first order kinetics. $k_{\text{obs}} = 1.3 \times 10^{-2} \text{ s}^{-1}$.

In addition, reaction kinetics of **HKPerox-Red** were investigated. Time courses of fluorescence intensities of **HKPerox-Red** (10 μ M) at 602 nm upon treatment with 100 μ M H_2O_2 were recorded. The reaction was almost completed within 10 min (Fig. S1, ESI†), meaning that a short period of incubation is enough to trigger a significant fluorescence response. At pH 8.0, this reaction could be further accelerated, which is consistent with the mechanism of tandem Payne/Dakin reaction. The reaction rate constant was calculated to be $1.3 \times 10^{-2} \text{ s}^{-1}$, based on a pseudo first order model by mixing 1 μ M **HKPerox-Red** with 1 mM H_2O_2 (Fig. 1e and f).

As shown in Fig. 2a, the absorption peak at 375 nm of **HKPerox-Ratio** was shifted to 425 nm upon H_2O_2 oxidation, which is consistent with restoration of ICT process in this ratiometric probe.^{12a,14} To our delight, subsequent fluorescence measurements revealed an isosbestic point on the fluorescence spectra of **HKPerox-Ratio** (Fig. 2b), indicating its clean conversion. The green fluorescent compound was also confirmed by UPLC-MS analysis to be the cleavage product 4-amino-1,8-naphthalimide (Scheme 2b and ESI†). The ratios of fluorescence emission intensities at 540 nm and 475 nm (F_{540}/F_{475}) were proportional to H_2O_2 concentrations ranging from 0 to 100 μ M. The selectivity of **HKPerox-Ratio** was also tested, which exhibited a 12.7-fold increase in F_{540}/F_{475} toward H_2O_2 , while other ROS/RNS gave negligible ratio changes (Fig. 2d). This reaction also proceeded rapidly to complete in 30 min (Fig. S2, ESI†). Collectively, these results demonstrate excellent water-solubility, sensitivity, selectivity of **HKPerox-Ratio** toward H_2O_2 .

Encouraged by their excellent performances toward H_2O_2 in chemical system, we further performed biological evaluations of **HKPerox-Red** and **HKPerox-Ratio** in living cells. The cytotoxicities of **HKPerox-Red** and **HKPerox-Ratio** were assessed in RAW264.7 macrophages, and no obvious toxicity was observed up to 20 μ M after 24 h incubation (Fig. S3 and S4, ESI†).

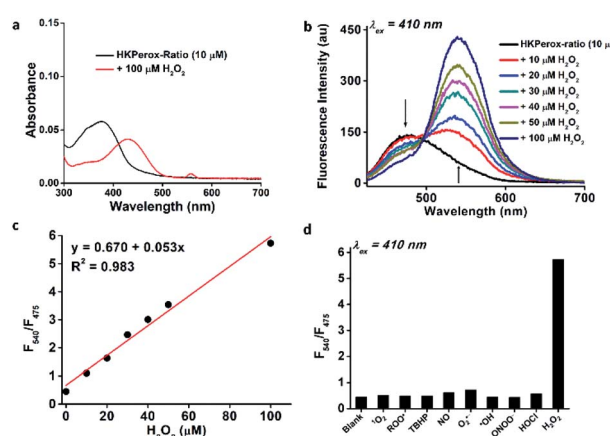


Fig. 2 Chemical characterization of **HKPerox-Ratio** (10 μ M) in 0.1 M potassium phosphate buffer (pH 7.4, 0.1% DMF, 100 μ M CCl_3CN). (a) Absorbance spectra of **HKPerox-Ratio** before and after treatment with H_2O_2 (100 μ M). (b) Fluorescence emission spectra of **HKPerox-Ratio** upon treatment with different amounts of H_2O_2 (0–100 μ M). (c) Ratios of the emission intensities (F_{540}/F_{475}) of **HKPerox-Ratio** as a function of H_2O_2 (0–100 μ M). (d) Fluorescence responses of **HKPerox-Ratio** toward ROS/RNS (100 μ M).



Molecular imaging of endogenous H_2O_2 production in live cells and *in vivo* using HKPerox-Red

We went on to apply **HKPerox-Red** in live cell imaging to detect endogenous H_2O_2 production with confocal microscopy. RAW264.7 macrophages were co-incubated with **HKPerox-Red** (4 μM) in Hank's Balanced Salt Solution (HBSS) for 30 min before imaging. As expected, the fluorescence signal in PMA treated cells was significantly stronger than that of untreated cells (Fig. 3a). This PMA induced H_2O_2 burst could be effectively inhibited by the addition of NADPH oxidase (NOX) inhibitor DPI, and quantifications based on imaging showed a clear 7-fold enhancement of fluorescence intensities (Fig. 3b). Endogenous H_2O_2 bursts can be robustly visualized in stimulated macrophages with **HKPerox-Red** in a selective manner.

We next explored the applications of **HKPerox-Red** to *in vivo* imaging of zebrafish. To perform molecular imaging of H_2O_2 produced in living zebrafish, the desirable probe should be both lipophilic and water-soluble to penetrate through fish skin by simple co-incubation. **HKPerox-Red**, our resorufin-derived H_2O_2 probe, featuring small-molecular weight, good lipophilicity, excellent water-solubility, and most importantly, ultra-sensitivity, is very promising for such study.

In our initial study, zebrafish embryos 6 hours post fertilization (hpf) were acquired to co-incubate with **HKPerox-Red** (including 100 μM CCl_3CN in 1 mL E3 buffer) or **HKPerox-2**, our previous rhodol-base probe,^{10a} at room temperature for 30 min to monitor zebrafish development process. Endogenous H_2O_2 produced during cell proliferation was clearly visualized by **HKPerox-Red** since the red fluorescence was detected inside zebrafish embryo (Fig. 4), while there was no fluorescence signal in the yolk part of the fertilized egg or outside of the embryo. In contrast, **HKPerox-2** could not penetrate through the embryo membrane *via* co-incubation, and the resulting fluorescence signals were only found outside the embryo. Thus, **HKPerox-Red** could efficiently stain zebrafish embryo by simple co-incubation, and H_2O_2 production during cell proliferation in early stage of embryo development was visualized.

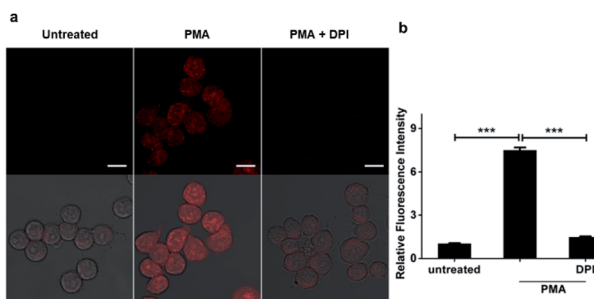


Fig. 3 Molecular imaging of endogenous hydrogen peroxide in living cells. (a) Representative confocal images for RAW264.7 macrophages co-incubated with **HKPerox-Red** (4 μM) and CCl_3CN (100 μM) in the absence or presence of PMA (200 ng mL^{-1}) or PMA plus DPI (100 nM). (b) Relative mean fluorescence intensities of cells incubated with **HKPerox-Red** were quantified. Scale bars represent 10 μm . Data are mean \pm SEM, $n = 30\text{--}34$ cells. Statistical significance was determined as *** $p < 0.001$ by Student's *t* test. PMA: phorbol 12-myristate 13-acetate; DPI: diphenyleneiodonium.

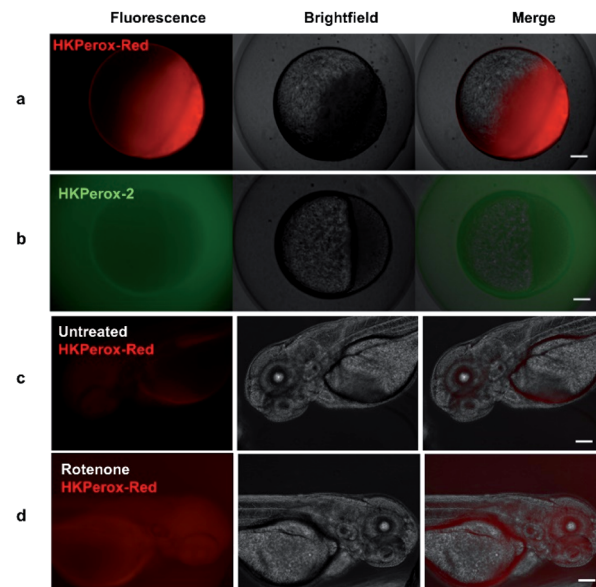


Fig. 4 Molecular imaging of endogenous H_2O_2 in 6 hpf zebrafish embryos with (a) **HKPerox-Red** (20 μM) and (b) **HKPerox-2** (20 μM). Molecular imaging of (c) untreated or (d) rotenone induced H_2O_2 in 72 hpf zebrafish embryos with **HKPerox-Red** (20 μM). Scale bars represent 100 μm .

Rotenone is a widely used pesticide that interferes with the electron transport chain during mitochondrial respiration. Previous study reveals that long term exposure to rotenone is associated with higher risk of Parkinson's disease in farm workers,¹⁵ while their models for rotenone challenging mainly focused on isolated mitochondria or cell lines,¹⁶ and the imaging reagents used to quantify ROS burst were traditional unselective probes. Thus, we applied **HKPerox-Red** to evaluate the effect of rotenone on zebrafish embryos. 72 hpf zebrafish embryos were incubated with **HKPerox-Red** (20 μM) for 20 min at room temperature, then challenged with or without rotenone (50 μM) in E3 buffer supplemented with 100 μM CCl_3CN for 15 min. Basal H_2O_2 production and distribution could be visualized as a weak fluorescence signal (Fig. 4c). However, this signal was significantly stronger in rotenone treated zebrafish, which indicates acute H_2O_2 burst in living embryos. Distributions of H_2O_2 burst could be found in the brain and gut regions of zebrafish embryos, which may further contribute to oxidative damage of proteins and the initiation of neurodegenerative diseases.

New assay development based on **HKPerox-Red**

As H_2O_2 is a biologically important oxidizing reagent, its production and scavenging profiles are of great interest in health products, nutrition, and food industry.¹⁷ Moreover, H_2O_2 is one of the most common products of enzyme catalyzed oxidations, thus a series of metabolites including glucose, cholesterol, uric acid, and sarcosine could be converted to H_2O_2 quantitatively with corresponding oxidases or enzyme mimetics.¹⁸

For example, in Amplex Red Glucose/Glucose Oxidase assay, glucose could be oxidized to glucuronolactone in the presence



of glucose oxidase and oxygen, and one equivalent of H_2O_2 is produced and quantified by Amplex Red in this process. However, this resulting fluorescence could be bleached by extra amounts of H_2O_2 in presence of horseradish peroxidase (HRP), and Amplex Red is also vulnerable to photo oxidation.^{6,19}

Similar to Amplex Red in both excitation and emission wavelengths, **HKPerox-Red** can be a novel molecular tool compatible with current assays using Amplex Red, yet it is more stable, sensitive, and HRP independent. In **HKPerox-Red** glucose assay, various amounts of glucose (0–40 μM , final concentrations) were added into potassium phosphate buffer, and then 1 U mL^{-1} glucose oxidase and **HKPerox-Red** (10 μM ; with 100 μM CCl_3CN) were added subsequently into the solution. Resulting solutions were incubated for 30 min at 37 °C before fluorescence measurement. As shown in Fig. 5a, H_2O_2 produced by glucose oxidation could be sensitively detected with **HKPerox-Red**, and a linear relationship between glucose concentrations and fluorescence emissions at 602 nm was observed. The detection limit of glucose was calculated to be as low as 34 nM ($3\sigma/k$) according to the calibration curve.

To prove the practical applications of this novel assay, non-diabetic urine and serum samples were analyzed by **HKPerox-Red** glucose assay, and only 1 μL serum is needed due to the ultra-sensitivity. In this experiment, 1 μL deproteinized serum was diluted with 1 mL potassium phosphate buffer (pH 7.4, 0.5% DMF) containing 1 U mL^{-1} glucose oxidase, 10 μM **HKPerox-Red** and 100 μM CCl_3CN . Quantifications were based on serum samples spiked with 3 mM glucose as internal standard, and the glucose concentration in serum sample was quantified as 4.38 ± 0.32 mM. Therefore, with tiny amount of sample, **HKPerox-Red** holds great potential to measure serum

glucose in a fast, accurate, and high-throughput assay. The ultrasensitivity also makes it possible to conduct non-invasive glucose evaluation with samples like sweat, saliva or tears. More importantly, **HKPerox-Red** enables a general assay for biologically important metabolites detection with suitable oxidases. As a proof of concept, uric acid/urate oxidase assay and sarcosine/sarcosine oxidase assay were developed by using **HKPerox-Red** (Fig. 5c and d), which provide practical methods for disease diagnosis based on metabolite screening. A clinical study with **HKPerox-Red** is on-going to use urinary sarcosine as potential biomarker for prostate cancer diagnosis.

Ratiometric detection of H_2O_2 burst in As_2O_3 treated leukaemia cells by using flow cytometry

Next, we sought to explore ratiometric H_2O_2 sensing with our **HKPerox-Ratio**. Although some H_2O_2 ratiometric fluorescent probes have been developed for this purpose, very few of them are sensitive enough to be used in flow cytometry, and none of them is suitable for quantifying endogenous H_2O_2 in living cells.¹³ We firstly applied **HKPerox-Ratio** in flow cytometry to detect H_2O_2 fluxes in leukemia cells challenged with As_2O_3 , a very effective approach to treat acute promyelocytic leukemia.²⁰ As leukemia cells are suspension cells, they are not suitable for confocal imaging; however, flow cytometry enables quantitative analysis of a large population of suspension cells rapidly. Moreover, with a suitable ratiometric probe, multiple fluorescence emissions could be detected simultaneously by flow cytometry,²¹ and the green to blue emission ratio ($F_{\text{green}}/F_{\text{blue}}$) reported by **HKPerox-Ratio** is expected to be a more reliable ratiometric indicator of cellular H_2O_2 .

For this purpose, U-937, NB4 and THP-1 leukemia cells were selected for the treatment with As_2O_3 for 24 h, and then untreated cells and As_2O_3 challenged cells were co-incubated with **HKPerox-Ratio** (10 μM) for 30 min before flow cytometry analysis. Over 10 000 cells were analysed, and $F_{\text{green}}/F_{\text{blue}}$ in each individual cell was calculated by a FlowJo software. As shown in Fig. 6a–c, As_2O_3 -treated leukemia cells could be clearly distinguished from those untreated cells by $F_{\text{green}}/F_{\text{blue}}$ ratio (x-axis), which correlates with H_2O_2 levels. Further quantifications in Fig. 6d showed a significant enhancement in $F_{\text{green}}/F_{\text{blue}}$ ratio in all three cell lines (1.9-fold for U-937, 1.7-fold for NB4, and 2.8-fold for THP-1), indicating a robust cellular H_2O_2 flux. This As_2O_3 -challenged H_2O_2 burst may be responsible for differentiation or apoptosis of leukemia cells.²² To conclude, **HKPerox-Ratio** is a promising probe to detect H_2O_2 fluxes via flow cytometry in a ratiometric manner, which provides an ideal platform to screen novel apoptosis inducer for leukemia therapy.

Ratiometric fluorescence imaging of starvation induced H_2O_2 in living cells

As H_2O_2 is believed to be an important mediator during autophagy in response to nutrient shortage,²³ we would like to identify and quantify endogenous H_2O_2 production during this process with ratiometric probe **HKPerox-Ratio**. RAW264.7 macrophages were co-incubated with **HKPerox-Ratio** (5 μM) in

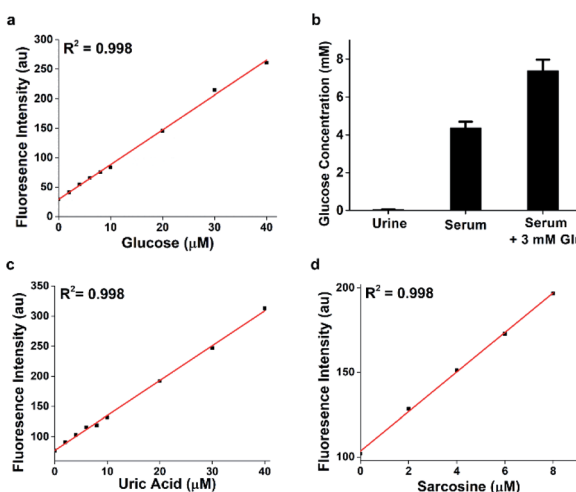


Fig. 5 (a) Ultrasensitive detection of glucose with **HKPerox-Red** (10 μM) in aqueous buffer (pH 7.4, 0.5% DMF, 1 U mL^{-1} glucose oxidase, 100 μM CCl_3CN). Excitation was provided at 565 nm; fluorescence emission was obtained at 602 nm. (b) Glucose quantifications of urine and serum samples using **HKPerox-Red** glucose assay. Data are mean \pm SEM, $n = 3$. (c) Detection of uric acid with **HKPerox-Red** (10 μM , with 1 U mL^{-1} urate oxidase) in aqueous buffer. (d) Detection of sarcosine with **HKPerox-Red** (10 μM , with 1 U mL^{-1} sarcosine oxidase) in aqueous buffer.



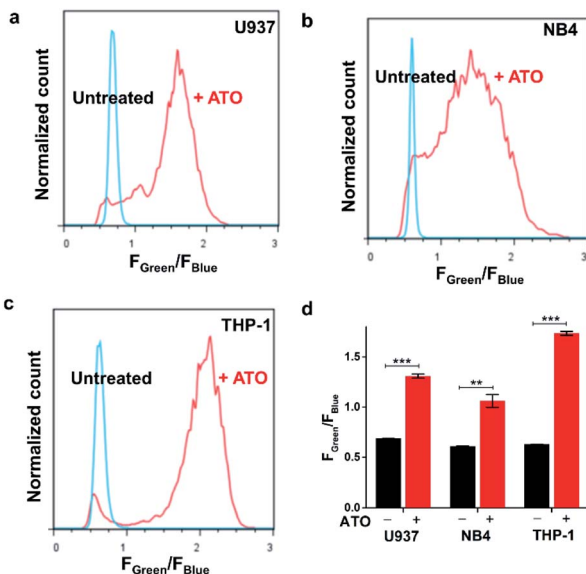


Fig. 6 Detection of arsenic trioxide induced H_2O_2 in leukemia cells with flow cytometry. (a) U937, (b) NB4, and (c) THP-1 cells were treated with or without $20 \mu\text{M} \text{As}_2\text{O}_3$ for 24 h, and then cells were incubated with **HKPerox-Ratio** ($10 \mu\text{M}$) and CCl_3CN ($100 \mu\text{M}$) for 30 min before flow cytometry analysis. The y-axis is the normalized cell count; the x-axis is the $F_{\text{green}}/F_{\text{blue}}$ ratio in each cell. (d) Fluorescence intensities ratios $F_{\text{green}}/F_{\text{blue}}$ in untreated cells and As_2O_3 treated cells were compared. Data are mean \pm SEM, $n = 3$ independent experiments. Statistical significance was determined as $**p < 0.01$, $***p < 0.001$ by Student's *t* test.

HBSS supplemented with $100 \mu\text{M} \text{CCl}_3\text{CN}$ for 30 min at 37°C with 5% CO_2 before confocal imaging. The fluorescence signals in blue region (440–490 nm) and green region (540–650 nm) were collected simultaneously with an excitation at 405 nm (Fig. 7a and b). As expected, the blue emission was significantly stronger than the green emission in untreated cells, and the merged Fig. 7c showed the predominant blue emission. In Fig. 7d, a heatmap of green-to-blue emission ratio ($F_{\text{green}}/F_{\text{blue}}$) was generated by a Ratio Plus plugin in ImageJ software. Basal H_2O_2 concentrations and distributions were reported as a small value of $F_{\text{green}}/F_{\text{blue}}$ (~ 0.2), which is consistent with low H_2O_2 levels in resting cells. To mimic starvation induced stress, RAW264.7 cells were incubated HBSS (protein free) for 24 h, and then confocal images were taken under the same optical settings. Upon starvation challenge, blue emission in cells decreased significantly, while green emission increased due to H_2O_2 burst (Fig. 7e and f). The merged image in Fig. 7g showed a predominant green emission, and the ratiometric heatmap (Fig. 7h) confirmed a significant increase of $F_{\text{green}}/F_{\text{blue}}$ (~ 1.0) inside the cells.

Quantification based on confocal images was performed to show a clear 5-fold overall increase of $F_{\text{green}}/F_{\text{blue}}$ in starvation-challenged cells compared to resting cells (Fig. 7i), which demonstrated the excellent sensitivity of **HKPerox-Ratio** in cell imaging. The green signal and blue signal overlapped well with an overlap coefficient of 0.85 (Fig. S5, ESI†), which shows a good co-localization of **HKPerox-Ratio** and its cleavage product in cells. Collectively, those data demonstrate that **HKPerox-Ratio**

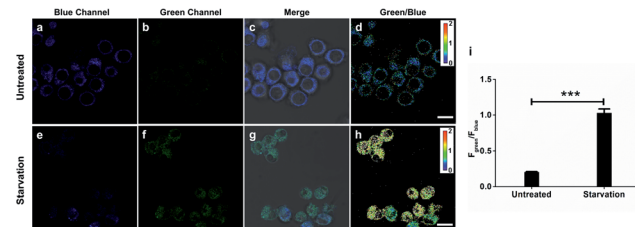


Fig. 7 Confocal images of H_2O_2 production with **HKPerox-Ratio** ($5 \mu\text{M}$) in untreated or nutrient-depleted (HBSS treatment) RAW264.7 macrophages. (a) and (e) Representative fluorescence images in the blue channel (440–490 nm). (b) and (f) Representative fluorescence images in the green channel (540–650 nm). (c) and (g) Merged images of blue, green and brightfield channels. (d) and (h) Pseudo-color heatmap of green/blue emission ratio ($F_{\text{green}}/F_{\text{blue}}$). (i) $F_{\text{green}}/F_{\text{blue}}$ of RAW 264.7 macrophages under homeostasis or starvation was quantified. Data are mean \pm SEM, $n = 19$ –29 cells. Statistical significance was determined as $***p < 0.001$ by Student's *t* test. Scale bars represent $10 \mu\text{m}$.

can be robustly applied in ratiometric imaging of endogenous H_2O_2 fluxes with spatio-temporal precision.

Quantitative measurement of cellular H_2O_2 by flow cytometry with live cell calibration

Calibration curves of previous ratiometric probes were largely established in a cell-free solvent/buffer mixture, which may not be applicable for precise quantification of cellular H_2O_2 .¹³ Therefore, we further applied **HKPerox-Ratio** in flow cytometry for quantitative measurement of H_2O_2 fluxes during starvation. As shown in Fig. 8a and b, a calibration curve with excellent linearity ($R^2 = 0.993$) was obtained by adding known amounts of H_2O_2 (0, 10, 20, 40, and $80 \mu\text{M} \text{H}_2\text{O}_2$) into the probe solution and then co-incubating with cells for 30 min before flow cytometry measurement. The green to blue emission ratio ($F_{\text{green}}/F_{\text{blue}}$) in each group of cells was analysed, and those cell populations could be distinguished in Fig. 8a. The detection limit of **HKPerox-Ratio** by flow cytometry measurement was estimated to be as low as $1.8 \mu\text{M}$ ($3\sigma/k$) in this cellular assay. A standard curve ($y = 0.372 + 0.010x$) with live cell calibration was thus established for RAW264.7 cells, enabling the direct measurement of intracellular H_2O_2 concentrations.

As shown in Fig. 8c and d, starvation induced H_2O_2 was detected and quantified with **HKPerox-Ratio**. Our data showed that 3 h starvation already induced a discernible increase in $F_{\text{green}}/F_{\text{blue}}$ ratio, corresponding to $7.9 \mu\text{M} \text{H}_2\text{O}_2$ according to the calibration curve. This rapidly elevated cellular H_2O_2 levels during starvation suggest that treatment of cells in protein-free buffers (such as HBSS and phosphate-buffered saline) may stimulate unexpected ROS burst, thus longtime incubation in those buffers should be avoided.

Moreover, H_2O_2 fluxes in living RAW264.7 cells reached its maximum concentration ($34 \mu\text{M}$) after 14 h starvation, and longer period of starvation (e.g. 24 h) did not induce higher levels of H_2O_2 . This endogenous H_2O_2 burst is sufficient to signal subsequent pathological processes, such as growth arrest or apoptosis.²⁴

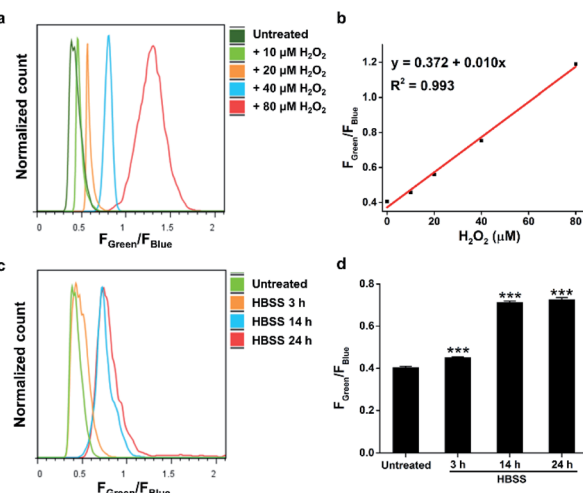


Fig. 8 Measurements of H_2O_2 concentrations in nutrient-depleted (HBSS treatment) RAW264.7 macrophages by flow cytometry analysis. (a) Histogram of the $F_{\text{Green}}/F_{\text{Blue}}$ ratio in RAW264.7 cells co-incubated with **HKPerox-Ratio** (10 μM) and CCl_3CN (100 μM) pretreated with 0, 10, 20, 40, and 80 μM H_2O_2 . (b) Calibration curve of $F_{\text{Green}}/F_{\text{Blue}}$ in RAW264.7 cells as a function of H_2O_2 concentrations. (c) Histogram of the $F_{\text{Green}}/F_{\text{Blue}}$ ratio in untreated or starvation challenged RAW264.7 cells incubated with **HKPerox-Ratio** (10 μM) and CCl_3CN (100 μM). (d) Comparison of $F_{\text{Green}}/F_{\text{Blue}}$ in untreated or starvation challenged cells. Data are mean \pm SEM, $n = 3$ independent experiments. Statistical significance was determined as *** $p < 0.001$ by Student's t test.

Due to variations of cellular environment, independent calibration curves should be obtained in different cell types before ratiometric H_2O_2 quantification. We further applied this protocol to HeLa cells, and a new calibration curve with excellent linearity ($y = 0.606 + 0.013x$, $R^2 = 0.988$) was obtained with **HKPerox-Ratio** by using flow cytometry (Fig. S6, ESI†). Note that the calibration curve obtained by using a fluorospectrometer in chemical system (Fig. 2c, $y = 0.670 + 0.053x$) is very different from those obtained by using flow cytometry with live cell calibration. This result indicates that calibration curves established in a cell-free solvent/buffer mixture are not applicable to cellular H_2O_2 measurement; however, with a suitable ratiometric probe, flow cytometry provides an ideal high-throughput platform for quantitative analysis. One potential risk from live cell calibration may arise from different cell permeabilities of **HKPerox-Ratio** and its cleavage product. A control experiment is recommended to co-stain the cells with both compounds to confirm their similar permeability (Fig. S7, ESI†). To the best of our knowledge, **HKPerox-Ratio** is the first ratiometric probe that can be used to quantify cellular H_2O_2 level by flow cytometry, which makes it an invaluable tool for not only qualitative detection, but also quantification in redox biology.

Conclusions

During past decades, great efforts have been made to develop novel H_2O_2 sensors, and diverse roles of H_2O_2 in mediating various biological processes have been uncovered. However, unambiguous quantitative analysis of H_2O_2 *in vitro* and *in vivo*

still represents a substantial challenge even to date. In this work, we have developed a pair of highly selective and sensitive fluorescent probes for precise measurement of H_2O_2 . Our unique strategy relies on tandem Payne/Dakin reaction, which provides a general and biocompatible strategy to distinguish H_2O_2 from other potential competing ROS. **HKPerox-Red** and **HKPerox-Ratio** have been successfully applied to evaluate the effects of PMA, As_2O_3 , rotenone, and starvation in various models.

In particular, **HKPerox-Red** with outstanding permeability could be used in zebrafish imaging by simple co-incubation, and rotenone induced oxidative stress was also successfully visualized *in vivo*. Moreover, the outstanding performance of **HKPerox-Red** has been exploited to develop new assays for H_2O_2 scavenging capacity or H_2O_2 -based quantification for metabolites including glucose, uric acid and sarcosine, which are regarded as diagnostic biomarkers for diabetes, gout, and prostate cancer, respectively. The intrinsic sensitivity of our novel strategy ensures its robust application for *in vitro* quantification of H_2O_2 and related metabolites.

Even more challenging in the redox biology field is to measure intracellular H_2O_2 accurately. In this study, we have developed **HKPerox-Ratio**, a small-molecule ratiometric probe, that allows quantitative detection of H_2O_2 by measuring the ratio of the blue and green emission. **HKPerox-Ratio** could be used in various cell lines with simple co-incubation, and the significant signal changes triggered by intracellular H_2O_2 were robustly captured by both flow cytometry and confocal imaging. Therefore, As_2O_3 -induced H_2O_2 fluxes in multiple leukemia cells were readily detected. **HKPerox-Ratio** further enables the first quantitative detection of endogenously generated H_2O_2 in living cells by using flow cytometry and live cell calibration curve.

We anticipate that both probes provide important molecular tools to study H_2O_2 physiology and pathology, and more efforts are on-going to apply **HKPerox** series probes and tandem Payne/Dakin reaction in advanced bio-imaging, drug screening, and disease diagnostics.

Conflicts of interest

S. Y., J. J. H., and D. Y. have filed a patent application for the reported probes.

Acknowledgements

The study using zebrafish embryos up to 72 hpf was strictly conducted according to the approved protocols provided by Zebrafish Core Facility at HKU and Committee on the Use of Live Animals and Teaching and Research (CULATR) at HKU (Hong Kong, China). We thank the HKU Li Ka Shing Faculty of Medicine Faculty Core Facility for support in confocal imaging, flow cytometry analysis, and zebrafish imaging. This work was supported by The University of Hong Kong, Morningside Foundation, Hong Kong Research Grants Council Area of Excellence Scheme (AoE/P-705/16) and National Natural Science Foundation of China (21961142011).



Notes and references

1 (a) K. Apel and H. Hirt, *Annu. Rev. Plant Biol.*, 2004, **55**, 373–399; (b) M. P. Murphy, *Biochem. J.*, 2009, **417**, 1–13.

2 (a) M. Reth, *Nat. Immunol.*, 2002, **3**, 1129–1134; (b) M. Giorgio, M. Trinei, E. Migliaccio and P. G. Pelicci, *Nat. Rev. Mol. Cell Biol.*, 2007, **8**, 722–728; (c) E. A. Veal, A. M. Day and B. A. Morgan, *Mol. Cell*, 2007, **26**, 1–14.

3 G. Filomeni, D. De Zio and F. Cecconi, *Cell Death Differ.*, 2015, **22**, 377–388.

4 (a) P. C. Panus, R. Radi, P. H. Chumley, R. H. Lillard and B. A. Freeman, *Free Radical Biol. Med.*, 1993, **14**, 217–223; (b) X. Liu and J. L. Zweier, *Free Radical Biol. Med.*, 2001, **31**, 894–901; (c) L. C. Seaver and J. A. Imlay, *J. Bacteriol.*, 2001, **183**, 7182–7189; (d) E. Werner, *Sci. Signaling*, 2003, **2003**, 13; (e) X. Li, Y. Liu, A. Zhu, Y. Luo, Z. Deng and Y. Tian, *Anal. Chem.*, 2010, **82**, 6512–6518; (f) N. Zhang, W. Ma, P.-G. He and Y.-T. Long, *J. Electroanal. Chem.*, 2015, **739**, 197–201.

5 (a) M. C. Chang, A. Pralle, E. Y. Isacoff and C. J. Chang, *J. Am. Chem. Soc.*, 2004, **126**, 15392–15393; (b) M. Abo, Y. Urano, K. Hanaoka, T. Terai, T. Komatsu and T. Nagano, *J. Am. Chem. Soc.*, 2011, **133**, 10629–10637; (c) P. Gao, W. Pan, N. Li and B. Tang, *Chem. Sci.*, 2019, **10**, 6035–6071; (d) K. J. Bruemmer, S. W. M. Crossley and C. J. Chang, *Angew. Chem., Int. Ed.*, 2020, **59**, 13734–13762.

6 (a) B. C. Dickinson and C. J. Chang, *Nat. Chem. Biol.*, 2011, **7**, 504–511; (b) X. H. Li, X. H. Gao, W. Shi and H. M. Ma, *Chem. Rev.*, 2014, **114**, 590–659; (c) Z. Guo, S. Park, J. Yoon and I. Shin, *Chem. Soc. Rev.*, 2014, **43**, 16–29; (d) F. Rezende, R. P. Brandes and K. Schröder, *Antioxid. Redox Signaling*, 2017, **29**, 585–602; (e) J. Huang, J. Li, Y. Lyu, Q. Miao and K. Pu, *Nat. Mater.*, 2019, **18**, 1133–1143; (f) X. Bai, K. K.-H. Ng, J. J. Hu, S. Ye and D. Yang, *Annu. Rev. Biochem.*, 2019, **88**, 605–633.

7 (a) V. V. Belousov, A. F. Fradkov, K. A. Lukyanov, D. B. Staroverov, K. S. Shakhbazov, A. V. Terskikh and S. Lukyanov, *Nat. Methods*, 2006, **3**, 281–286; (b) D. S. Bilan, L. Pase, L. Joosen, A. Y. Gorokhovatsky, Y. G. Ermakova, T. W. J. Gadella, C. Grabher, C. Schultz, S. Lukyanov and V. V. Belousov, *ACS Chem. Biol.*, 2013, **8**, 535–542; (c) B. Morgan, K. Van Laer, T. N. E. Owusu, D. Ezeriña, D. Pastor-Flores, P. S. Amponsah, A. Tursch and T. P. Dick, *Nat. Chem. Biol.*, 2016, **12**, 437–443; (d) T. F. Langford, B. K. Huang, J. B. Lim, S. J. Moon and H. D. Sikes, *Nat. Commun.*, 2018, **9**, 3145; (e) V. V. Pak, D. Ezeriña, O. G. Lyublinskaya, B. Pedre, P. A. Tyurin-Kuzmin, N. M. Mishina, M. Thauvin, D. Young, K. Wahni, S. A. Martínez Gache, A. D. Demidovich, Y. G. Ermakova, Y. D. Maslova, A. G. Shokhina, E. Eroglu, D. S. Bilan, I. Bogeski, T. Michel, S. Vriz, J. Messens and V. V. Belousov, *Cell Metab.*, 2020, **31**, 642–653.

8 (a) E. W. Miller, A. E. Albers, A. Pralle, E. Y. Isacoff and C. J. Chang, *J. Am. Chem. Soc.*, 2005, **127**, 16652–16659; (b) B. C. Dickinson and C. J. Chang, *J. Am. Chem. Soc.*, 2008, **130**, 9638–9639; (c) A. R. Lippert, G. C. V. De Bittner and C. J. Chang, *Acc. Chem. Res.*, 2011, **44**, 793–804; (d) L. Yuan, W. Lin, Y. Xie, B. Chen and S. Zhu, *J. Am. Chem. Soc.*, 2012, **134**, 1305–1315; (e) X. Sun, S.-Y. Xu, S. E. Flower, J. S. Fossey, X. Qian and T. D. James, *Chem. Commun.*, 2013, **49**, 8311–8313; (f) J. Wang, W. Zhu, G. Niu, G. Jiang, Q. Chen, P. Gao, Y. Li, G. Zhang, X. Fan and B. Z. Tang, *Chem. Commun.*, 2018, **54**, 13957–13960; (g) Y. Zhang, C. Yan, C. Wang, Z. Guo, X. Liu and W.-H. Zhu, *Angew. Chem., Int. Ed.*, 2020, **59**, 9059–9066.

9 X. Xie, X. e. Yang, T. Wu, Y. Li, M. Li, Q. Tan, X. Wang and B. Tang, *Anal. Chem.*, 2016, **88**, 8019–8025.

10 (a) S. Ye, J. J. Hu and D. Yang, *Angew. Chem., Int. Ed.*, 2018, **57**, 10173–10177; (b) S. Ye, N. Hananya, O. Green, H. Chen, A. Q. Zhao, J. Shen, D. Shabat and D. Yang, *Angew. Chem., Int. Ed.*, 2020, **59**, 14326–14330.

11 D. Pham, U. Basu, I. Pohorilets, C. S. Croix, S. C. Watkins and K. Koide, *Angew. Chem., Int. Ed.*, 2020, **59**, 17435–17441.

12 (a) D. Srikun, E. W. Miller, D. W. Domaille and C. J. Chang, *J. Am. Chem. Soc.*, 2008, **130**, 4596–4597; (b) C. Chung, D. Srikun, C. S. Lim, C. J. Chang and B. R. Cho, *Chem. Commun.*, 2011, **47**, 9618–9620; (c) Y. Wen, K. Liu, H. Yang, Y. Li, H. Lan, Y. Liu, X. Zhang and T. Yi, *Anal. Chem.*, 2014, **86**, 9970–9976; (d) B. Dong, X. Song, X. Kong, C. Wang, Y. Tang, Y. Liu and W. Lin, *Adv. Mater.*, 2016, **28**, 8755–8759; (e) W. Zhang, T. Liu, F. Huo, P. Ning, X. Meng and C. Yin, *Anal. Chem.*, 2017, **89**, 8079–8083; (f) H. Wang, Z. He, Y. Yang, J. Zhang, W. Zhang, P. Li and B. Tang, *Chem. Sci.*, 2019, **10**, 10876–10880; (g) Z. Wang, X. Ai, Z. Zhang, Y. Wang, X. Wu, R. Haindl, E. K. L. Yeow, W. Drexler, M. Gao and B. Xing, *Chem. Sci.*, 2020, **11**, 803–811.

13 D. Andina, J.-C. Leroux and P. Luciani, *Chem.-Eur. J.*, 2017, **23**, 13549–13573.

14 (a) Z. Xu, J. Yoon and D. R. Spring, *Chem. Commun.*, 2010, **46**, 2563–2565; (b) Z.-Z. Li, C.-G. Niu, G.-M. Zeng, Y.-G. Liu, P.-F. Gao, G.-H. Huang and Y.-A. Mao, *Sens. Actuators, B*, 2006, **114**, 308–315; (c) V. S. Lin, W. Chen, M. Xian and C. J. Chang, *Chem. Soc. Rev.*, 2015, **44**, 4596–4618; (d) Y. Hu, X. Li, Y. Fang, W. Shi, X. Li, W. Chen, M. Xian and H. Ma, *Chem. Sci.*, 2019, **10**, 7690–7694.

15 M. T. Caroline, F. Kamel, G. W. Ross, A. H. Jane, M. G. Samuel, M. Korell, C. Marras, S. B. Grace, M. Kasten, R. C. Anabel, K. Comyns, B. R. Marie, C. Meng, B. Priestley, H. F. Hubert, F. Cambi, M. U. David, A. Blair, P. S. Dale and J. W. Langston, *Environ. Health Perspect.*, 2011, **119**, 866–872.

16 (a) S. C. Sousa, E. N. Maciel, A. E. Vercesi and R. F. Castilho, *FEBS Lett.*, 2003, **543**, 179–183; (b) C. M. Testa, T. B. Sherer and J. T. Greenamyre, *Mol. Brain Res.*, 2005, **134**, 109–118; (c) N. Yadava and D. G. Nicholls, *J. Neurosci.*, 2007, **27**, 7310–7317.

17 (a) M. Özyürek, B. Bektaşoğlu, K. Güçlü, N. Güngör and R. Apak, *J. Food Compos. Anal.*, 2010, **23**, 689–698; (b) N. Higashi, H. Yokota, S. Hiraki and Y. Ozaki, *Anal. Chem.*, 2005, **77**, 2272–2277.

18 M. E. Hafez, H. Ma, W. Ma and Y.-T. Long, *Angew. Chem., Int. Ed.*, 2019, **58**, 6327–6332.

19 (a) K. J. Reszka, B. A. Wagner, C. P. Burns and B. E. Britigan, *Anal. Biochem.*, 2005, **342**, 327–337; (b) B. Zhao, F. A. Summers and R. P. Mason, *Free Radical Biol. Med.*, 2012, **53**, 1080–1087.

20 (a) G. Q. Chen, J. Zhu, X. G. Shi, J. H. Ni, H. J. Zhong, G. Y. Si, X. L. Jin, W. Tang, X. S. Li, S. M. Xong, Z. X. Shen, G. L. Sun, J. Ma, P. Zhang, T. D. Zhang, C. Gazin, T. Naoe, S. J. Chen, Z. Y. Wang and Z. Chen, *Blood*, 1996, **88**, 1052–1061; (b) G. Q. Chen, X. G. Shi, W. Tang, S. M. Xiong, J. Zhu, X. Cai, Z. G. Han, J. H. Ni, G. Y. Shi, P. M. Jia, M. M. Liu, K. L. He, C. Niu, J. Ma, P. Zhang, T. D. Zhang, P. Paul, T. Naoe, K. Kitamura, W. Miller, S. Waxman, Z. Y. Wang, H. de The, S. J. Chen and Z. Chen, *Blood*, 1997, **89**, 3345–3353.

21 (a) A. Kaur, M. A. Haghighatbin, C. F. Hogan and E. J. New, *Chem. Commun.*, 2015, **51**, 10510–10513; (b) Y. Chen, C. Zhu, J. Cen, Y. Bai, W. He and Z. Guo, *Chem. Sci.*, 2015, **6**, 3187–3194.

22 (a) K. Kinjo, M. Kizaki, A. Muto, Y. Fukuchi, A. Umezawa, K. Yamato, T. Nishihara, J. Hata, M. Ito, Y. Ueyama and Y. Ikeda, *Leukemia*, 2000, **14**, 431–438; (b) E.-K. Noh, H. Kim, M. J. Park, J. H. Baek, J.-H. Park, S. J. Cha, J.-H. Won and Y. J. Min, *Leuk. Res.*, 2010, **34**, 1501–1505.

23 (a) Y. Chen, E. McMillan-Ward, J. Kong, S. J. Israels and S. B. Gibson, *Cell Death Differ.*, 2008, **15**, 171–182; (b) M. Dewaele, H. Maes and P. Agostinis, *Autophagy*, 2010, **6**, 838–854; (c) J. Lee, S. Giordano and J. H. Zhang, *Biochem. J.*, 2012, **441**, 523–540.

24 (a) F. Antunes and E. Cadenas, *Free Radical Biol. Med.*, 2001, **30**, 1008–1018; (b) Q. M. Chen, J. Liu and J. B. Merrett, *Biochem. J.*, 2000, **347**, 543–551.

